

Continuous-wave mid-infrared frequency conversion in silicon nanowaveguides

Ryan K. W. Lau,^{1,*} Michaël Ménard,² Yoshitomo Okawachi,¹ Mark A. Foster,¹
Amy C. Turner-Foster,² Reza Salem,³ Michal Lipson,^{2,4} and Alexander L. Gaeta¹

¹*School of Applied and Engineering Physics, Cornell University, Ithaca, New York 14853, USA*

²*School of Electrical and Computer Engineering, Cornell University, Ithaca, New York 14853, USA*

³*PicoLuz, 10335 Guilford Road, Jessup, Maryland 20794, USA*

⁴*Kavli Institute at Cornell for Nanoscale Science, Cornell University, Ithaca, New York 14853, USA*

*Corresponding author: rkl48@cornell.edu

Received November 15, 2010; revised February 1, 2011; accepted February 28, 2011;
posted March 9, 2011 (Doc. ID 138146); published March 30, 2011

We report the first demonstration of cw wavelength conversion from the telecommunications band to the mid-IR (MIR) region via four-wave mixing in silicon nanowaveguides. We measure a parametric bandwidth of 748 nm by converting a 1636 nm signal to produce a 2384 nm idler and show continuously tunable wavelength conversion from 1792 to 2116 nm. This report indicates that the advantages of silicon photonics may be leveraged to create devices for a large range of MIR applications that require cw operation. © 2011 Optical Society of America
OCIS codes: 190.4380, 190.4390, 320.7100.

Integrated silicon photonics provides a potential platform for the realization of all-optical signal processing functionality for high-speed telecommunications networks. The high refractive index and large third-order nonlinearity of silicon enable efficient nonlinear optical interactions at relatively low power levels [1–3]. Furthermore, dispersion engineering of silicon nanowaveguides has allowed broadband parametric gain and wavelength conversion via four-wave mixing (FWM) in compact, complementary-metal-oxide-semiconductor-compatible devices [3,4]. While many useful all-optical devices based on FWM in silicon have been demonstrated in the telecommunications band [3–9], the parametric gain and frequency conversion efficiency are fundamentally limited by the nonlinear optical loss mechanisms of two-photon absorption (TPA) and the resulting free-carrier absorption (FCA). It has been shown that the TPA coefficient decreases with increasing wavelength beyond 1.7 μm and drops to zero for wavelengths beyond 2.2 μm, which corresponds to half of the bandgap energy of silicon [10]. As a result, silicon photonic devices designed to operate beyond 2.2 μm have exhibited relatively large amplification [11]. Consequently, the advantages of silicon photonic technology may be extended to the mid-IR (MIR) region to create chip-scale devices for applications such as infrared spectroscopy, biochemical sensing, free-space communications, and astronomy [12–14].

Previous demonstrations of MIR FWM in silicon nanowaveguides have used a pulsed pump source [11,15]. However, there are a number of applications, such as free-space communications and high-precision spectroscopy, where the use of a cw pump is desirable since it facilitates wavelength conversion of a continuous data stream and can transfer any amplitude and phase modulation from the signal to the idler, which allows for the creation of modulated signals at MIR wavelengths where modulators are not readily available. In this Letter, we report what we believe to be the first demonstration of broadband, cw FWM in silicon nanowaveguides with a pump near 2 μm. We achieve wavelength conversion over 748 nm and generation of an idler wave at 2384 nm. In

addition, we show continuously tunable conversion across 320 nm, which was limited only by the availability of signal sources.

In order to predict the MIR FWM performance in the silicon nanowaveguides, we use the following coupled differential equations for the pump A_P , signal A_S , and idler A_I fields:

$$\frac{dA_P}{dz} = -\frac{1}{2} \left[\alpha_{\text{lin}}^P + \beta_{\text{TPA}} I_P + \alpha_{\text{FCA}}^P I_P^2 \right] A_P + i\gamma |A_P|^2 A_P, \quad (1.1)$$

$$\frac{dA_S}{dz} = -\frac{1}{2} \left[\alpha_{\text{lin}}^S + 2\beta_{\text{TPA}} I_P + \alpha_{\text{FCA}}^S I_P^2 \right] A_S + 2i\gamma |A_P|^2 A_S + \gamma A_P^2 A_I^* \exp(i\Delta kz), \quad (1.2)$$

$$\frac{dA_I}{dz} = -\frac{1}{2} \left[\alpha_{\text{lin}}^I + 2\beta_{\text{TPA}} I_P + \alpha_{\text{FCA}}^I I_P^2 \right] A_I + 2i\gamma |A_P|^2 A_I + \gamma A_P^2 A_S^* \exp(i\Delta kz), \quad (1.3)$$

where $I_P = n_P c |A_P|^2 / 2$ is the pump intensity; α_{lin}^P , α_{lin}^S , and α_{lin}^I are the linear propagation loss coefficients at the pump, signal, and idler, respectively; β_{TPA} is the TPA coefficient at the pump wavelength; $\Delta k = 2\gamma |A_P|^2 - (2k_P - k_S - k_I)$ is the phase mismatch; k_P , k_S , and k_I are the wavenumbers of the pump, signal, and idler, respectively; $\gamma = 2\pi n_2 / \lambda_P A_{\text{eff}}$ is the effective nonlinearity of the nanowaveguide; n_2 is the nonlinear index coefficient; λ_P is the pump wavelength; and A_{eff} is the effective area of the propagating mode. The FCA coefficient α_{FCA} due to TPA is given by [16]

$$\alpha_{\text{FCA}} = 1.45 \times 10^{-21} [\text{m}^2] \left(\frac{\lambda_P}{1.55 \times 10^{-6} [\text{m}]} \right)^2 \left(\frac{\beta_{\text{TPA}} \tau_{\text{eff}} \lambda_P}{2hc} \right), \quad (2)$$

where τ_{eff} is the effective free-carrier lifetime, h is Planck's constant, c is the speed of light in vacuum, and all the numeric quantities are given in meters.

The group-velocity dispersion (GVD) of the nanowaveguides can be modeled using a custom finite-difference mode solver, and, by using this value, we numerically integrate Eqs. (1.1), (1.2), and (1.3) to determine the optimal dimensions for the maximum conversion bandwidth. Figure 1 shows the simulated GVD for the fundamental TE polarization mode of the nanowaveguides with varying cross sections. The widths range from 940 to 970 nm, and the height is fixed at 280 nm. We find that a nanowaveguide cross section of 950 nm \times 280 nm will have a zero-GVD wavelength of 1950 nm, which is within the tuning range of our pump source.

Nanowaveguides were fabricated on a silicon-on-insulator wafer with a 3 μ m buried oxide and a 500 nm silicon layer. The silicon slab was thinned by wet oxidation, and the waveguides were patterned with electron-beam lithography before being dry etched with SF₆ chemistry and clad with 3 μ m of silicon oxide by plasma enhanced chemical vapor deposition. Inverted tapers narrowing to 250 nm were added at the input and output to improve the coupling efficiency [17]. The pump source is a high-power cw thulium fiber laser with a tuning range of 1940 to 1970 nm, and the signal source is a second cw thulium fiber laser, tunable from 1790 to 1930 nm. The TE polarization mode is selected for the pump and signal beams using a polarization beam-splitter cube and polarization controller, respectively. The pump and signal beams are combined with a pellicle beam splitter and coupled into the silicon nanowaveguide using an aspherical lens. The output of the waveguide is coupled through a lensed fiber and sent to an optical spectrum analyzer.

We fix the pump at 1950 nm and continuously tune the signal from 1790 to 1930 nm for each nanowaveguide to measure the conversion efficiency, defined here as the ratio of output idler power to output signal power. The nanowaveguide widths range from 940 to 970 nm, the heights are 280 nm, and the lengths are 1 cm. Figure 2 shows the theoretical and measured conversion efficiencies as functions of idler wavelength. By measuring the transmission of nanowaveguides with varying lengths,

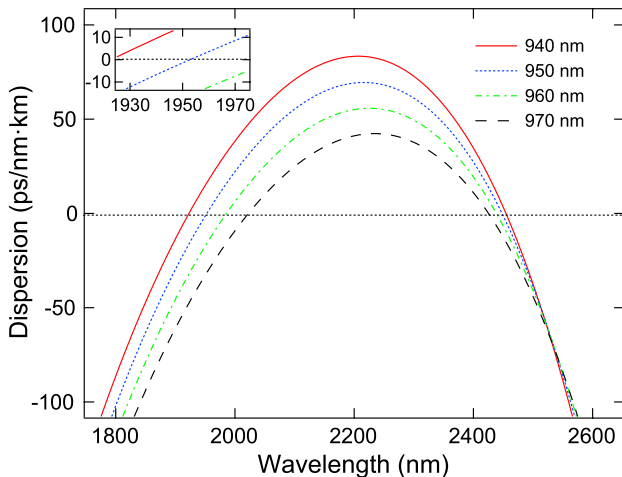


Fig. 1. (Color online) Simulated GVD curves for the TE mode of nanowaveguides with widths ranging from 940 to 970 nm and a fixed height of 280 nm. The inset shows that a nanowaveguide 950 nm wide will have a zero-GVD wavelength near 1950 nm.

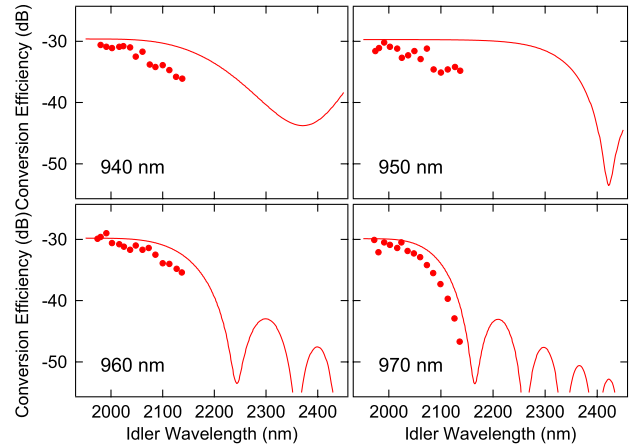


Fig. 2. (Color online) Theoretical (curves) and measured (dots) conversion efficiencies as functions of idler wavelength for nanowaveguides of varying widths. The heights and lengths are 280 nm and 1 cm, respectively. The cw pump is fixed at 1950 nm, and the signal is tuned from 1790 to 1930 nm. The measured peak conversion efficiency is approximately -30 dB.

we estimate the propagation loss and input/output coupling loss at the pump wavelength of 1950 nm to be -1.7 dB/cm and -3 dB/facet, respectively. We estimate the pump and signal power inside the nanowaveguides to be 30 mW and 300 μ W, respectively. At these powers, the measured peak conversion efficiency is approximately -30 dB, which is in good agreement with theoretical predictions. As we increase the pump power to approximately 160 mW, we measure a maximum conversion efficiency of -17.8 dB. Further increase of the pump power damaged the input tapers of the nanowaveguide, and at this time we have not been able to determine the source of damage. We have not seen significant pump saturation due to nonlinear losses at these pump powers.

We find that the maximum theoretical 3 dB conversion bandwidth occurs for a 940-nm-wide nanowaveguide pumped at 1940 nm. Figure 3 shows the theoretical and measured conversion efficiencies as functions of idler

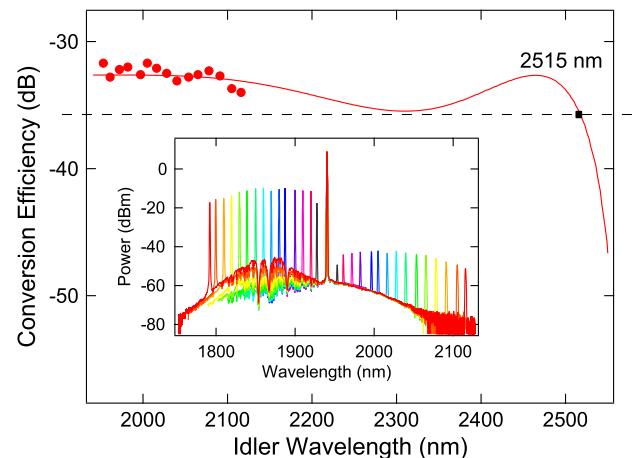


Fig. 3. (Color online) Theoretical (curve) and measured (dots) conversion efficiencies as functions of idler wavelength for a 940 nm \times 280 nm \times 1 cm nanowaveguide pumped at 1940 nm. The measured 3 dB conversion bandwidth is 324 nm, from 1792 to 2116 nm. The theoretical 3 dB conversion bandwidth is 936 nm, from 1579 to 2515 nm. The inset shows the measured FWM spectra.

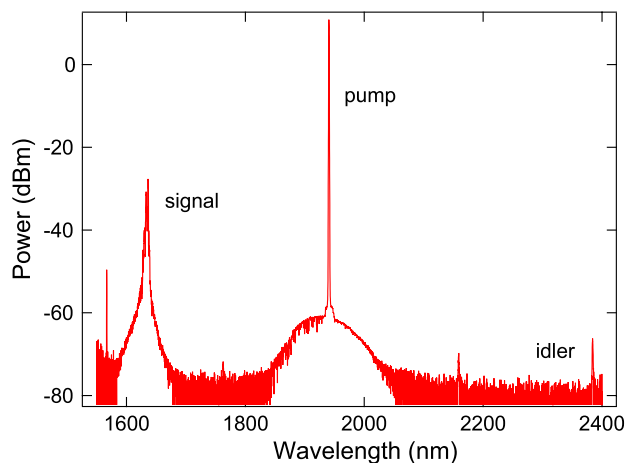


Fig. 4. (Color online) Measured FWM spectra showing broadband wavelength conversion across 748 nm. The signal, pump, and idler wavelengths are 1636, 1940, and 2384 nm, respectively.

wavelength. The inset shows the measured FWM spectra as the signal is tuned from 1792 to 1928 nm. The corresponding idler wavelength ranges from 1953 to 2116 nm. With approximately 25 mW of pump power, the conversion efficiency ranges from -31.7 to -34 dB, varying less than 3 dB across the entire tuning range of the signal. The measurable conversion bandwidth is 324 nm, currently limited by the wavelength range of our signal laser. Theoretically, the full 3 dB conversion bandwidth is 936 nm, from 1579 to 2515 nm. To confirm the large theoretical bandwidth, we use a U-band Fabry–Perot laser diode at 1636 nm as the cw signal source. Pumping with 25 mW at 1940 nm, we observe wavelength conversion to 2384 nm, demonstrating a conversion bandwidth of at least 748 nm. The FWM output spectrum showing the signal, pump, and idler is shown in Fig. 4. The conversion efficiency is -38.6 dB, which is slightly lower than predicted. We note that some of the discrepancy may be due to several approximations in our theoretical approach, as we do not model the dispersion of the effective nonlinearity or the mode size mismatch among the signal, pump, and idler fields. Also, the lower conversion efficiency may be partially attributed to coupling and propagation loss of the idler in the lensed fiber at the output of the nanowaveguide. In addition, we observe a spectral peak around 2158 nm, corresponding to the Stokes field arising from the spontaneous Raman scattering of the $2\ \mu\text{m}$ pump. The frequency difference between the Stokes and pump fields is measured to be 15.6 THz, the optical phonon frequency in silicon. The spectral peak around 1762 nm results from Raman-assisted FWM between the Stokes and pump fields [18]. The feature near 1550 nm corresponds to the pump used in the thulium fiber laser. The upper wavelength limit of our spectrum analyzer is $2.4\ \mu\text{m}$, and thus we have not been able to measure conversion to longer wavelengths.

In conclusion, we have designed and fabricated a silicon nanowaveguide with a zero-GVD wavelength near

$2\ \mu\text{m}$, enabling broadband cw parametric mixing in the MIR region. We observe continuously tunable wavelength conversion across 324 nm. Additionally, we generate a 2384 nm idler and measure a maximum conversion bandwidth of 748 nm, limited by the detection range of our spectrum analyzer. This demonstration indicates that integrated silicon photonics may be extended beyond the traditional telecommunications window and into a new realm of MIR applications.

We acknowledge support from the Defense Advanced Research Projects Agency (DARPA) under the Parametric Optical Processes and Systems (POPS) and Centers in Integrated Photonics Engineering Research (CIPhER) programs and by the Center for Nanoscale Systems, supported by the National Science Foundation (NSF) and New York State Foundation for Science, Technology and Innovation (NYSTAR). This work was performed in part at the Cornell NanoScale Facility, a member of the National Nanotechnology Infrastructure Network, which is supported by the NSF (Grant ECS-0335765).

References

1. Q. Lin, O. J. Painter, and G. P. Agrawal, *Opt. Express* **15**, 16604 (2007).
2. M. A. Foster, A. C. Turner, M. Lipson, and A. L. Gaeta, *Opt. Express* **16**, 1300 (2008).
3. R. L. Espinola, J. I. Dadap, R. M. Osgood, Jr., S. J. McNab, and Y. A. Vlasov, *Opt. Express* **13**, 4341 (2005).
4. K. Yamada, H. Fukuda, T. Tsuchizawa, T. Watanabe, T. Shoji, and S. Itabashi, *IEEE Photon. Technol. Lett.* **18**, 1046 (2006).
5. M. A. Foster, A. C. Turner, J. E. Sharping, B. S. Schmidt, M. Lipson, and A. L. Gaeta, *Nature* **441**, 960 (2006).
6. Y.-H. Kuo, H. Rong, V. Sih, S. Xu, M. Paniccia, and O. Cohen, *Opt. Express* **14**, 11721 (2006).
7. R. Salem, M. A. Foster, A. C. Turner, D. F. Geraghty, M. Lipson, and A. L. Gaeta, *Nat. Photon.* **2**, 35 (2007).
8. Y. Dai, Y. Okawachi, A. C. Turner-Foster, M. Lipson, A. L. Gaeta, and C. Xu, *Opt. Express* **18**, 333 (2009).
9. A. C. Turner-Foster, M. A. Foster, R. Salem, A. L. Gaeta, and M. Lipson, *Opt. Express* **18**, 1904 (2010).
10. A. D. Bristow, N. Rotenberg, and H. M. van Driel, *Appl. Phys. Lett.* **90**, 191104 (2007).
11. X. Liu, R. M. Osgood, Y. A. Vlasov, and W. M. J. Green, *Nat. Photon.* **4**, 557 (2010).
12. R. A. Soref, S. J. Emelett, and W. R. Buchwald, *J. Opt. A* **8**, 840 (2006).
13. V. Raghunathan, D. Borlaug, R. Rice, and B. Jalali, *Opt. Express* **15**, 14355 (2007).
14. L. Labadie and O. Wallner, *Opt. Express* **17**, 1947 (2009).
15. S. Zlatanovic, J. S. Park, S. Moro, J. M. Chavez-Boggio, I. B. Divliansky, N. Alic, S. Mookherjea, and S. Radic, *Nat. Photon.* **4**, 561 (2010).
16. R. Claps, V. Raghunathan, D. Dimitropoulos, and B. Jalali, *Opt. Express* **12**, 2774 (2004).
17. V. R. Almeida, R. Panepucci, and M. Lipson, *Opt. Lett.* **28**, 1302 (2003).
18. R. Claps, V. Raghunathan, D. Dimitropoulos, and B. Jalali, *Opt. Express* **11**, 2862 (2003).